Department of Energy

Office of Energy Efficiency and Renewable Energy

Solid State Lighting Core Technologies

Final Report

Award No. DE-EE0007624

Principal Investigator

Franky So

North Carolina State University

Department of Materials Science and Engineering

Raleigh, NC 27695

Phone: (919) 513 7060

E-mail: fso@ncsu.edu

1. Project Summary

The external quantum efficiency (EQE) of a planar OLED is limited to about 25% and about 75% of the light is trapped in the substrate, waveguided and SPP modes. In this project, we demonstrated that nanostructures can significantly improve the EQE of an OLED. The objective is to improve the EQE to 70% using corrugated substrates with an index contrast layer. We conducted optical studies of the operating devices using ARES measurements, and used the results to guide the design of corrugated substrates as well as the OLED stack for better performance.

During the first year of the program, we have demonstrated over 60% EQE in a corrugated green OLED with a macrolens for light extraction. By comparing the optical characteristics of OLEDs fabricated on single and polycrystal corrugated structures, we confirm that the enhancement using corrugated substrates comes from the waveguide and SPP modes extraction.

To push the device EQE to 70%, we conducted a systematic study of the corrugation based on its pitch, depth and profile. We developed a series of processes to precisely control the corrugation structure and observed that while an abrupt surface profile results in a stronger mode extraction, it also introduces a leakage current. On the other hand, a smooth profile are less efficient in mode extraction, it preserves the quality of an OLED. Based on these observations, we determine that a single crystal hole corrugation results in an optimum EQE with a low leakage current when the substrates are planarized with PEDOT. To improve the extraction of waveguided mode, we also introduce an index contrast layer (ICL) to enhance the diffraction efficiency at the corrugated ITO and glass interface. We optimized our recipe for the low index thin film processing and reduced its refractive index from 1.50 to 1.38. As a result, the optimized device shows 47.6% EQE, which is 1.64 times higher than the reference planar device. By extracting the substrate mode with a macrolens, we obtained an EQE of 71.6%, which is a 2.46 times enhancement. The cross-section SEM image reveals the high EQE is due to the formation of an air gap at the interface of the ICL, resulting in an increase of the index contrast to $\Delta n \sim 1$. We use angle-resolved electroluminescence spectroscopy (ARES) to demonstrate that the ICL improves the extraction of the TM, TE waveguide and SPP mode more efficiently leading to the observed high efficiency.

For compatibility with large area OLED panels, we also studied the optical properties of external microlens arrays (MLAs) on a corrugated substrate. We address the directional emission issue with single crystalline microlens arrays (MLAs) by fabricating polycrystalline MLAs. The process uses a colloidal assembly method to create a monolayer of silica spheres, then uses PDMS

stamps to replicate the pattern for multi-use imprinting. The MLAs are close-packed in short range but have random orientations in the long range. This avoids stronger extraction along the optical axes of single crystal MLAs and prevents the directional emission issue. We also demonstrate that the color shift induced by the corrugation can be minimized using MLAs. In this scenario, the MLAs work as a diffuser to randomize the directional emission from the extracted waveguide and SPP modes. With these improvements, the design of corrugated OLED with polycrystal MLAs become more suitable for general lighting applications.

Milestones: All milestones are met.

Milestone Summary Table					
Task Number	Milestone Type and Description	Milestone Description	Start Quarter	End Quarter	Status
1	Fabrication of corrugated substrates and corrugation Profile	Periodicity of 0.5 µm and depth 70 nm	M1	M06	Completed
1	Fabrication of corrugated substrates OLED device performance	Leakage current of 50 nA/cm^2	M1	M12	Completed
2	Use of low index material and its properties	Index < 1.2	M7	M12	Completed
2	Use of low index material and its optical transmittance	Optical transmittance of 90%	M7	M12	Completed
3	OLED on low index buffer layer and corrugation profile	Periodicity of 0.5 µm and depth 70 nm	M13	M18	Completed
3	OLED on low index buffer layer and device performance	EQE of 70% with macrolens	M13	M24	Completed
4	Microlens profile and OLED with microlens array	Periodicity of 1 µm	M7	M15	Completed
4	Device performance of OLED with microlens array	EQE enhancement of 80%	M13	M18	Completed
4	Device performance of OLED with microlens array + low index material	EQE of 70%	M16	M24	Completed

2. Motivation for the Project

Internal quantum efficiency values of OLEDs have reached nearly 100%. However, the external quantum efficiency (EQE) of typical OLEDs is approximately 25%. This low efficiency is due to the 70% trapped lights trapped in substrate modes, waveguide modes and SPP modes. Several methods including corrugated structures in OLED can improve the outcoupling efficiency by extracting the waveguided mode as well as the SPP mode. An additional increase EQE can be achieved by incorporating an index contrast layer in the device, which enhances the diffraction efficiency at the ITO/glass interface and improves the overall outcoupling efficiency.

3. Introduction to Optical Modes

A lot of work has been devoted to improving the performance of OLEDs and, as a result, the internal quantum efficiency values of OLEDs have reached nearly 100%. However, the external quantum efficiency (EQE) of typical OLEDs is approximately 20%. The remaining ~80% of photons are trapped in substrate modes (~20%) because of the total internal reflection at the surface of glass substrate and waveguide modes (~15%). (Figure 1)

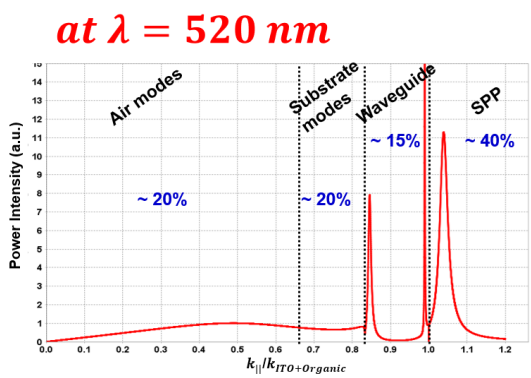

Figure 1. Distribution of OLED emission into different modes.

Substrates Modes

Figure 2 shows a simplified structure of bottom emitting OLEDs. Light that is generated in an organic film should pass through the transparent substrate to be seen by human eyes. However, when light travels from the higher refractive index medium to the lower refractive index medium, light that strikes the interface between two mediums at an angle larger than a certain angle will be entirely reflected. Glass is usually used as a substrate for OLEDs and its refractive index is 1.5 which is higher than the refractive index of air (n_{air}=1). Thus, some portion of emitted light from

the organic layer will be waveguiding inside the glass substrate. These trapped lights are called as substrate modes.

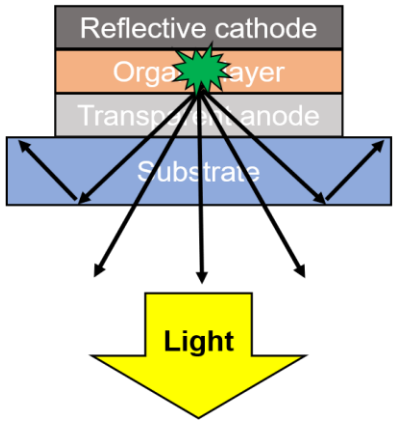

Figure 2. Schematic structures of a bottom emitting OLEDs with outcoupled light and trapped light inside the substrate

Waveguide Modes

Light propagating in the slab waveguide is described in Figure 3a. The interference between propagating off-axis plane waves is dependent on y-direction. Thus, we can think that the slab WG has a close analogy with Fabry Perot Etalon (Fig 3d). In Fabry Perot Etalon, the waves that do not satisfy the mode condition cannot exist inside the cavity. The quantized nature of WG modes results from constructive and destructive interference between propagating waves inside a device.

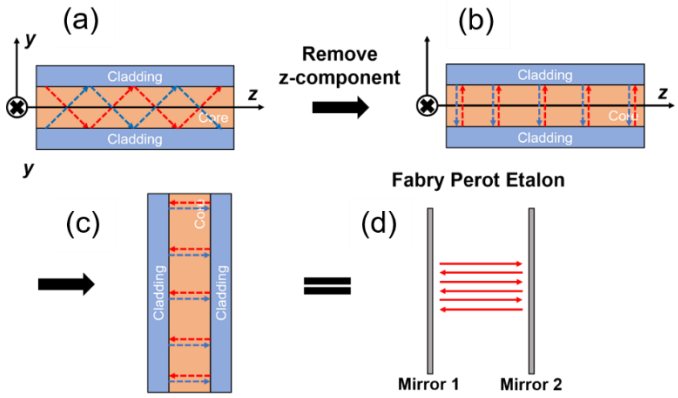

Figure 3. (a) Guided waves in a slab waveguide. (b) y-components of the guided waves in a slab waveguide. (c) A rotated slab waveguide. (d) The Fabry Perot Etalon

Another important thing is that there are two kinds of transverse modes in the slab WG. One is a transverse electric (TE) mode. The other is a transverse magnetic (TM) mode (Figure 4). These two modes generated by the Fresnel reflection at the interface. According to the Fresnel coefficient, when light is reflected at the interface, there is a phase shift, and this shift is dependent on the polarization state of waves and incident angle.[3] The reason of the polarization dependence of phase shift in Fresnel reflection can be qualitatively explained with evanescent field of the TIR. Evanescent fields are formed when waves experience TIR at the interface. P-polarized light has a y-component electric field so, it interacts more with the evanescent fields than s-polarized light. In other words, p-polarized light travels more into the evanescent field (outside of the boundary) than s-polarized light. This results in the phase difference between s- and p-polarized light after reflection at the interface. As a result, TE and TM modes cannot degenerate in the slab WG. Thus, we need to distinguish these two modes to describe how light travels inside OLEDs.

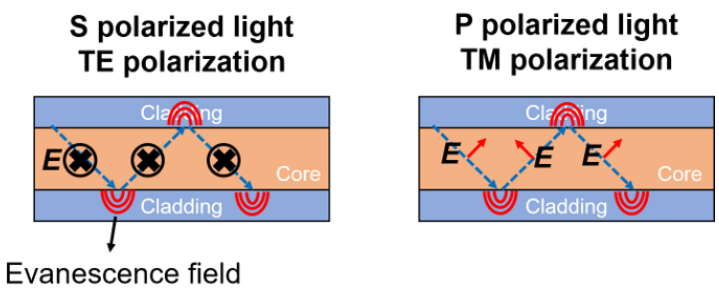

Figure 4. Illustration of TE and TM polarization of guided modes in a slab waveguide.

Surface Plasmon Polariton Modes

As can be known from the Figure 5a, at the surface of a metal, the electric fields caused by electron charge density fluctuation have both perpendicular and parallel field components to the interface. Hence, the surface of a metal (more precisely, the interface between a metal and a dielectric) can support both transverse and longitudinal electric fields. The existence of the transverse components implies that the surface plasmons of metals or doped semiconductors can interact directly with lights. The coupled system between the photon and surface plasmons called as surface plasmon polariton (SPP).

Only p-polarized waves can be coupled to SPP modes. This is because the electric field component in s-polarized light is parallel to the surface of a medium, so it cannot interact with the plasma at the surface of the medium. Thus, SPP modes only support TM modes. The light coupled into SPP modes will travel along the interface and decay exponentially (evanescent fields) into both dielectric and metal media (Figure 2.6b). By solving Maxwell's equation, the dispersion relation of SPP can be obtained, and it is given by:

$$k_{SPP}(\omega) = k_0\sqrt{\frac{\varepsilon_m\varepsilon_d}{\varepsilon_m+\varepsilon_d}} = \frac{\omega}{c}\sqrt{\frac{\varepsilon_m(\omega)\varepsilon_d(\omega)}{\varepsilon_m(\omega)+\varepsilon_d(\omega)}},$$

where k_0 is a vacuum wave vector, ε_m is a complex dielectric function of a metal, and ε_d is a complex dielectric function of a dielectric layer. k_{SPP} considers only in-plane wave vector (i.e., the component of wave vector, which is parallel to the interface). The dispersion curves for the SPPs and light in a dielectric medium are shown in Figure 5c. The x-axis in the graph is the in-plane wave vector and the y-axis is the frequency. As can be know from the dispersion curve in Figure 4c, the light line and the SPP curve do not intersect each other. Light coupled to SPP modes cannot be radiated into far-field. Therefore, SPP modes in OLEDs are regarded as a loss.

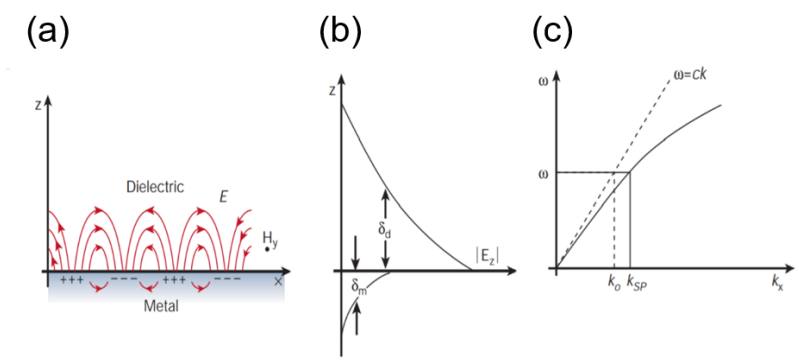

Figure 5. (a) Schematic illustration of plasma and its electric field at a metal surface. (b) Electric field distribution in the z-direction at the interface between a metal and dielectric. (c) SPP dispersion curve. (Figure from Barnes, W. L.; Dereux, A.; Ebbesen, T. W. Surface plasmon subwavelength optics. *Nature* **2003**, 424, 824.)

4. Light Extraction with Corrugation

Every point on a wavefront is a source of wavelets (Huygens' principle). Thus, when the propagating wave encounters the optical grating, point source radiator will be formed at each groove. Then newly generated waves at each groove will constructively or destructively interfere with each other. As a result, the propagation direction of the propagating wave changes (Figure 6a). This process is called diffraction and the direction of a diffracted ray can be calculated by the grating equation:[3]

$$a(\sin\theta_m - \sin\theta_i) = n\lambda,$$

where a is the pitch of grating, θ_m and θ_i is the angle of diffracted and incident ray with respect to interface normal, respectively, λ is a wavelengh of the ray, and n is an integer.

The propagation angle has limitations to describe the traveling light inside and outside the OLEDs device. Thus, in OLEDs research, the in-plane wave vector is commonly used to describe the light traveling inside and outside of the device. Therefore, the grating equation needs to be expressed with wave vector. The grating equation in reciprocal space is given by:[5]

$$\vec{k} = \vec{k}_0 + \vec{k}_g,$$

where $\vec{k}$ and $\vec{k}_0$ are the wavevectors of diffracted and incident ray, respectively and $\vec{k}_g$ is a grating vector, $\vec{k}_g = \frac{2\pi}{a}$. From the equation, we can know that the optical grating act as a momentum modulator for the waves that strike it.

The confined mode and grating are shown in Figure 6b. The in-plane wave vector of confined mode changes as it strikes the grating. However, since the total momentum of light should be conserved, z-component of wave vector also needs to be changed. As a result, the propagation direction of the confined mode changed and thus can escape to the outside.

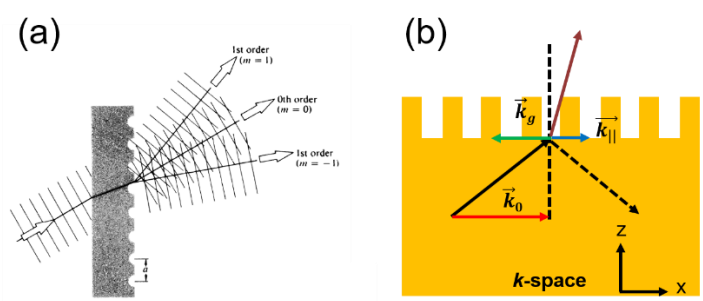

Figure 6. (a) Diffracted light by the optical grating.[3] (b) The out-coupled confined mode by the optical grating

Preparation of Corrugated Substrates

Corrugated substrates are prepared by nano-imprinting. Optical adhesive NOA 81 with a matching refractive index with glass (n = 1.5) was drop-casted on a planar glass substrate. Then a PDMS stamp carrying the negative form of the corrugated pattern was pressed onto the optical adhesive. The substrates were then treated with UV light (365 nm, 14 mW/cm^2) for 10 minutes to cross-link the adhesive and the pattern was preserved. Finally, the PDMS stamp was removed and the corrugated substrates were ready for OLED fabrication.

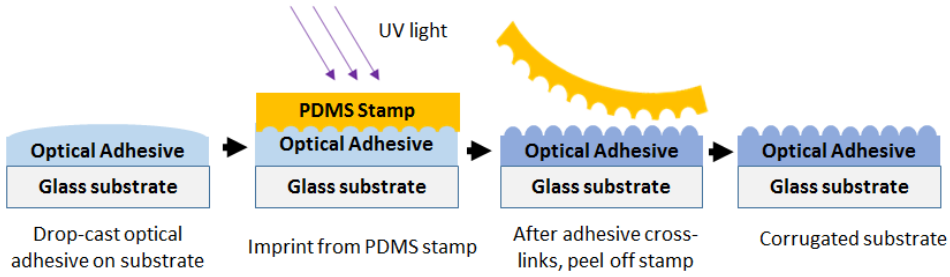

Figure 7. Preparation of corrugated glass substrate by soft imprinting

SEM images for some of the master molds used in this study are shown in Figure 8. Nano-structure arranged in hexagonal and square 2D patterns were prepared. The pitch values of the corrugation patterns varied from 300 nm to 2 µm, and the depth values vary from 80 nm to 500 nm. The corrugated poly crystal mold was fabricated via colloidal self-assembly to obtain the 2D polycrystal structure. A self-assembled silica beads monolayer was spread on the sapphire substrate surface, then the substrates were dry-etched to obtain a 2D poly crystal pattern (Fig 9). A proper amount of etching time was needed to obtain a dome-shaped pattern. We have successfully fabricated and studied the morphology of polycrystal corrugated patterns using a nanoimprinting method. The corrugated patterns have a pitch of 0.5 µm and a depth of 70 nm. To conduct a systematic study, we are also fabricating new corrugated molds with various pitches (0.3 ~ 0.8 µm).

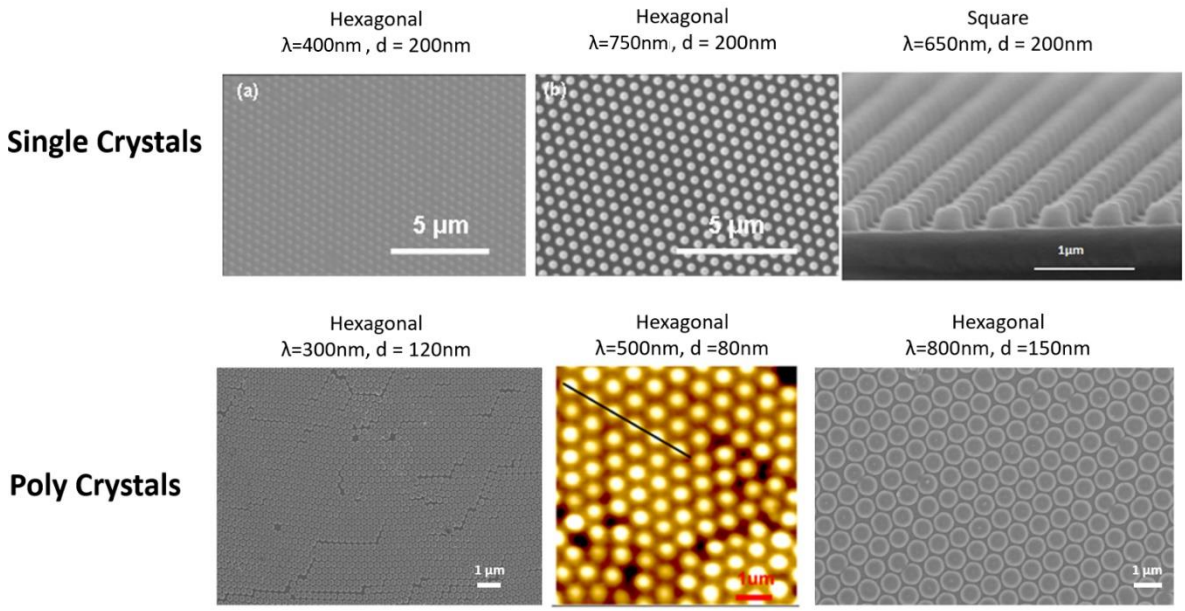

Figure 8. AFM and SEM images of master molds carrying corrugated patterns with different pitch (λ) and depth (d).

The variant corrugation profiles provide a good set of samples to study device light outcoupling, emission angular profile, and electrical stability. In this research, a green emitter $Ir(ppy)_2(acac)$ was used to fabricate bottom emitting OLEDs. The EL peak of $Ir(ppy)_2(acac)$ is at 520 nm, and a corrugation pattern with a comparable pitch (400 nm) as the peak wavelength and 80 nm depth were selected for device study.

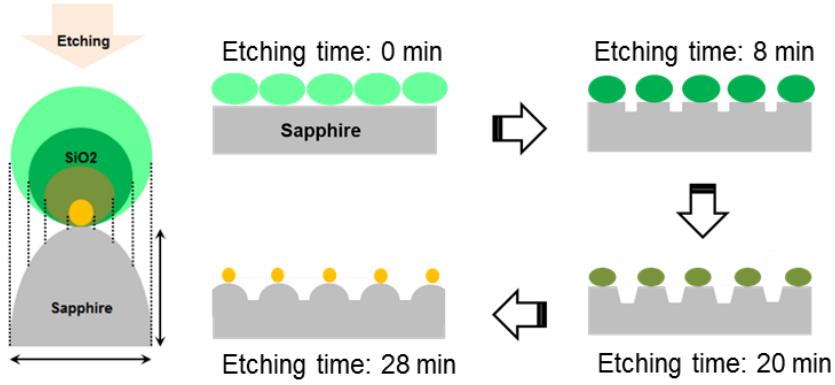

Figure 9. Schematic illustration of silica microsphere lithography process

OLED Fabrication and Optimization

After the glass substrates were prepared, a 100 nm thick ITO was sputtered as the transparent anode. Then the substrate was transferred to a a vacuum chamber for the OLED stack fabrication. The optimized planar device has the following structure: ITO(100 nm)/MoOx(10 nm)/TAPC(40 nm)/CBP:Ir(ppy)$_2$(acac)(30 nm,7% doping)/3TPYMB(20 nm)/NBphen(25 nm)/LiF(1 nm) /Al(100 nm). In this structure, TAPC is the hole transport layer, CBP doped with Ir(ppy)$_2$(acac) is the emitting layer, 3TPYMB is the hole and exciton blocking layer, NBphen is the electron transport layer.

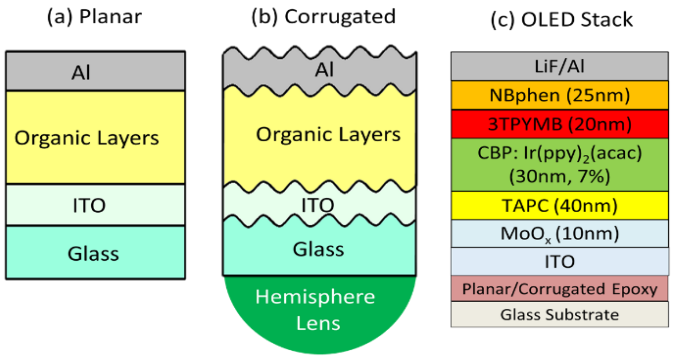

Figure 10. Device structure (a) planar (b) corrugated and (c) OLED stack

To maximize the efficiency, this device structure was optimized in several steps. Firstly, optical simulation software Setfos 4.4 was used to optimize the stack. The thickness of each layer was then optimized such that the light out-coupling is maximum. Then the device charge balance was optimized by changing the individual layer thickness of 3TPYMB and NBphen. At last the emitter doping ratio was optimized. Increasing the doping ratio results in reduced efficiency roll-off at high current density, but also causes lower peak efficiency and slight spectrum redshift. Therefore, an optimized doping ratio of 7% was selected.

To determine the light extraction properties of corrugated substrates, green OLED was fabricated on a corrugated glass substrate with a surface morphology shown in Fig 8 (a). The pitch of the corrugation was 400 nm, and the depth was 80 nm. The J-V-L, EL spectra and efficiency comparisons of optimized devices are plotted in Fig 11. From the J-V curve (Fig 11 (a)), the current density of corrugated device was seen to be higher than the planar device. This can be explained with reduced effective film thickness due to corrugation. The uneven surface caused by the corrugation also makes polishing less effective; therefore, the leakage current of corrugated device

is around 100 nA/cm^2. Note this leakage current level doesn't affect the device performance and stability.

The optimized planar device had a peak current efficiency (Fig 11 (b)) of 86 cd/A, and the corrugated device is 103 cd/A. The 20% enhancement in efficiency is attributed to the diffraction of waveguide modes and SPP mode by the corrugated structure, which shifts the in-plane wave vector towards air mode for extraction. However, the corrugation alone was not enough to extract all the light, and some trapped modes are diffracted but remain trapped in substrate mode. To extract the light trapped in the substrate, a hemispherical lens with a diameter of 15 mm and the same refractive index as the glass was attached to the back side of the substrate. The lens efficiently extracts substrate modes, doubles the efficiency of the corrugated device and result in ~60% EQE (Fig 11 (c)). The total enhancement from both corrugation and the half-ball lens is 2.7 times. Due to the quasi-periodic nature of the corrugated pattern, the enhancement in light extraction applies to a wide range of wavelength, and there is no distortion to the EL spectra (Fig 11 (d)).

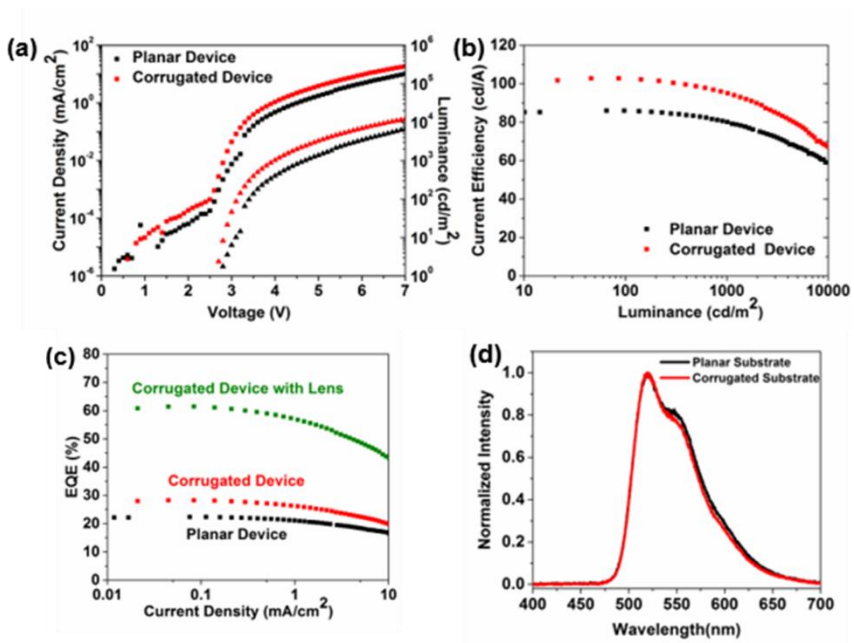

Figure 11. (a) J-V-L (b) current efficiency (c) EL spectra of OLED fabricated on planar and corrugated substrates. (d) Calculated EQE for planar (black), corrugated device (red) and corrugated device with lens attached (green).

5. Optical Study with Angle-Resolved EL Spectroscopy

Although high efficiencies have been reported with various corrugated structures, it is unclear which optical modes are extracted and how the extraction of different optical modes contributes to the outcoupling efficiency enhancement. Angle-resolved EL spectroscopy (ARES) can experimentally map out the air mode of an operating OLED, quantitatively identify the efficiency enhancement coming from the extraction of waveguide and SPP modes. The ARES analysis gives valuable guidance for designing optimum corrugated structures to realize high-efficiency devices.

The schematic drawing of an ARES setup is shown in Fig 12(a). The device to be measured was mounted on a rotation stage with an angular step < 1°. An Ocean Optics spectrometer collected the EL spectra at each viewing angle (θ). For polarized-ARES, a polarizer was inserted between the optical fiber and the device. When the polarizer axis was parallel to the optical table, only the P-light (TM) was transmitted; when the axis was perpendicular to the optical table, only S-light (TE) was transmitted. The photon energy (E) was determined by $E = hc/\lambda$; the in-plane wavevector was determined by $k_{//} = 2\pi/\lambda * \sin(\theta)$; the power density was determined by $I = I(EL)/\cos(\theta)$, where I(EL) is the power density determined from our Ocean Optics spectrometer, and the $1/\cos(\theta)$ factor takes into consideration the projected pixel area (Fig 12(b)).

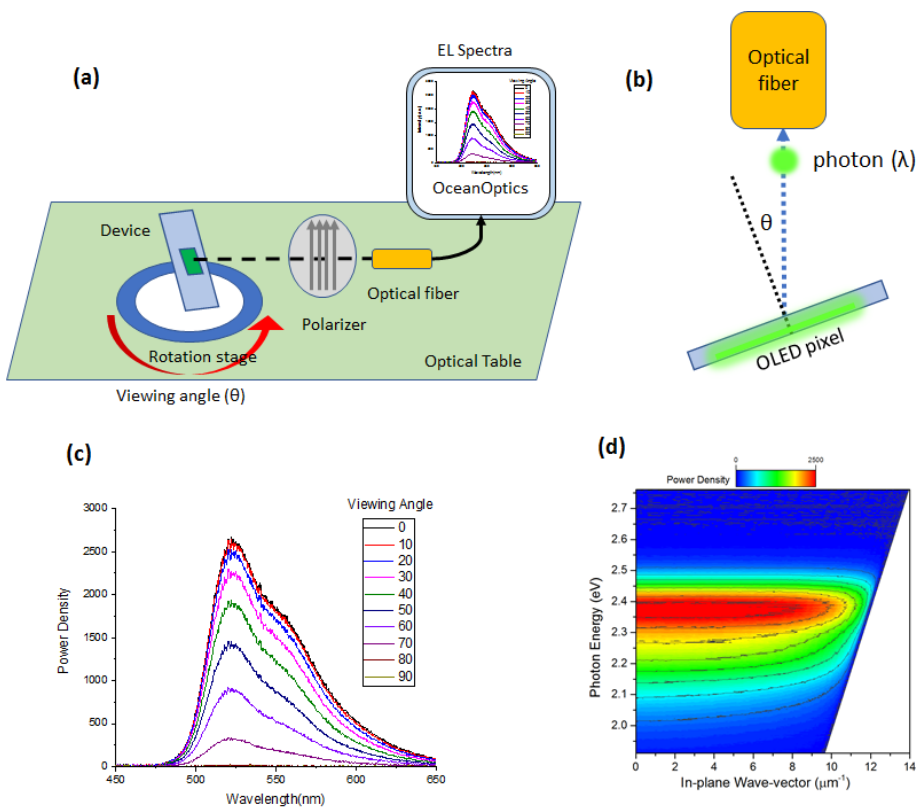

Figure 12. (a) Optical setup of ARES measurement. (b) Determination of the in-plane wave-vector ($k_{//}$) of a photon with a wavelength of λ. (c) Measured EL spectra of a planar OLED device at different viewing angles. (d) A sample of an ARES spectral profile.

For a planar OLED device using $Ir(ppy)_2acac$ as the emitter, its EL spectra from 0 to 90 degree viewing angles are shown in Fig 12(c). By plotting the calibrated power density (I) against the in-plane wave-vector ($k_{//}$) and photon energy, we obtained the ARES spectral profile as shown in Fig 12(d). Considering E = 2.38 eV, which corresponds to the emission peak of $Ir(ppy)_2acac$, the power density almost remains constant from $k_{//}$ = 0 to 9 μm^{-1}, indicating it is a Lambertian emission profile. At larger $k_{//}$ values, the transmittance from the glass substrate to air rapidly decreases, corresponding to a reduction in power density. When $k_{//}$ is larger than k_0 (12.08 μm^{-1}), photons cannot escape the OLED stack, which defines the edge of air cone.

ARES study provides important optical information related to the light extraction of an OLED device. To understand how corrugation interacts with photons emitted from an OLED, we fabricated OLEDs on both single and poly photonic crystal substrates and measured their ARES profiles. The ARES plots for planar and corrugated OLEDs (with single and polycrystal patterns) are shown in Fig 13. The single and poly photonic crystals both have a pitch of 400 nm.

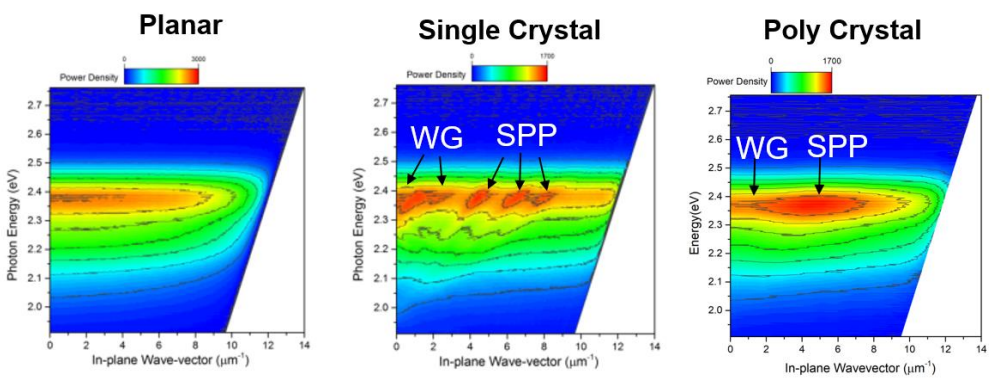

Figure 13. ARES plots of OLEDs on planar substrate, single crystal substrate and polycrystal substrate. For the single crystal device, the angle of measured incident plane and the optical axis of the photonic crystal (ϕ) is 5°

We compare the ARES profile of two corrugated devices with the planar device. The air mode background of the three devices was similar, showing a power distribution close to a Lambertian

emitter. On top of the background, the single crystal device showed multiple discrete features, which are associated with waveguide and SPP modes through diffraction wavevectors of the photonic crystal. The polycrystal device showed a continuous additional feature across a larger range of in-plane wavevectors, which is mostly contributed by SPP mode diffraction. The reason waveguide diffraction is weaker in the polycrystal devices can be attributed to the smoother change in the corrugation profile. The polycrystal substrate has a dome shape corrugation, while the single crystal substrate shows a rod shape corrugation (Fig 14). More abrupt change in surface morphology results in a stronger modulation of the refractive index, which leads to stronger diffraction of waveguide modes.

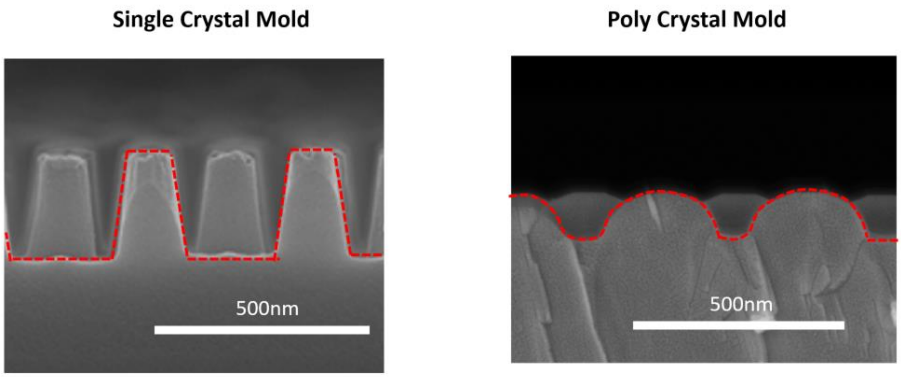

Figure 14. Cross section images of single and polycrystal molds. The red dash lines depict the corrugation profiles. Single crystal mold has a rod-shaped, abrupt profile, whereas poly crystal mold has a dome-shaped, smooth profile. The single crystal mold has a depth of 200 nm and the polycrystal mold has a depth of 120 nm. After imprinting, both corrugations are planarized to achieve a depth of 80 nm

Effect of Corrugation Profile on Optical and Electrical Properties

To study the effect of corrugation profile on diffraction efficiency, we fabricated both positive pattern (rod corrugation) and negative pattern (hole corrugation) glass substrates using only the same single crystal mold (400 nm pitch). These two corrugated substrates were further planarized using PEDOT to achieve the same corrugation depth of 80 nm. Corresponding SEM images of PEDOT planarized rod and hole substrates are given in Fig 15.

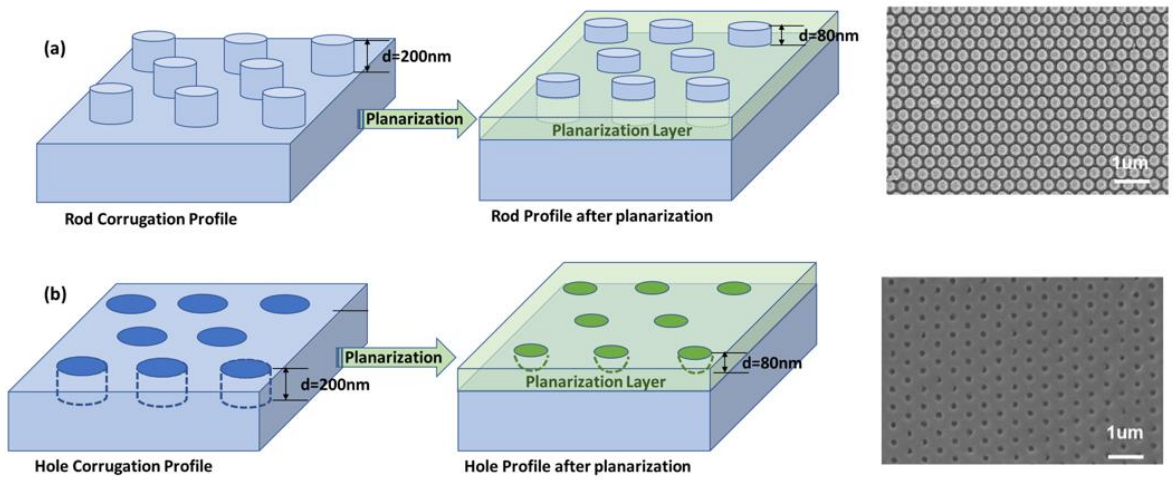

Figure 15. Schematic diagram of corrugated profiles of with (a) rod and (b) hole shaped corrugation and the corresponding SEM images.

The J-V and EQE plots for the planar OLED and OLEDs with rod and hole corrugation are shown in Fig 16. Below the device turn-on voltage (2.6 V), both the planar and hole corrugation OLEDs have low leakage currents, whereas the leakage current for rod corrugation OLED is one order of magnitude higher. This indicates the existence of shunt paths inside the rod shape corrugated OLED. These results indicate the electrical properties are also strongly affected by the shape of the corrugation. Corrugation with abrupt profile causes current to go through the sharp edges, which not only leads to higher leakage current, compromises the charge balance, but also stresses the emitters on the shunt paths, leading to a lower efficiency. This is also confirmed in the EQE plot, where hole corrugation device shows higher EQE than the planar device, and the rod corrugation device shows lower EQE.

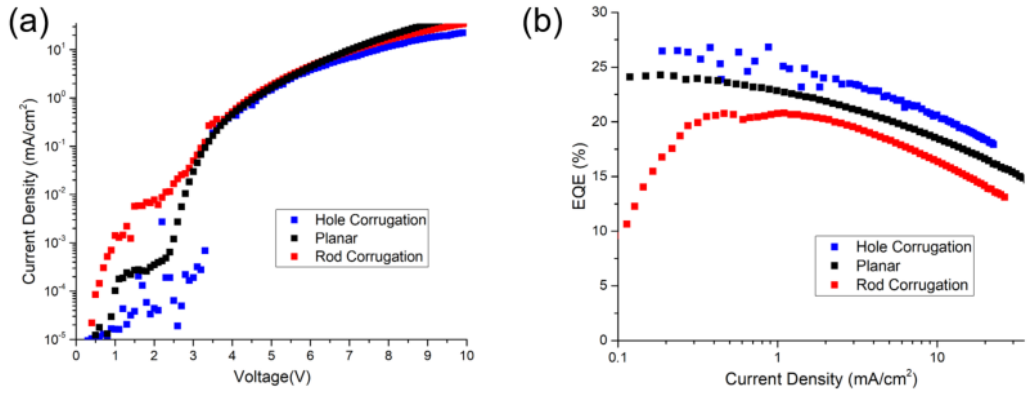

Figure 16. (a) J-V and (b) EQE plots of planar OLED, corrugated OLED on rod and hole corrugations

We also studied the optical characteristics of these two structures. The ARES plots of the hole and rod corrugation OLEDs are shown in Fig 17. The diffraction features are assigned to waveguide modes (close to air cone center) and SPP modes (further away from air cone center). The two devices are driven at the same current density; therefore, the ARES plot intensities can be directly compared. Between the two corrugation structures, the rod corrugation OLED has stronger waveguided and SPP diffraction intensity, but weaker air mode intensity. This observation confirms that the abrupt corrugation profile results in stronger diffraction, but the sharp rod profile also strongly affects the device efficiency by creating shunt paths. In this case, the overall efficiency is reduced.

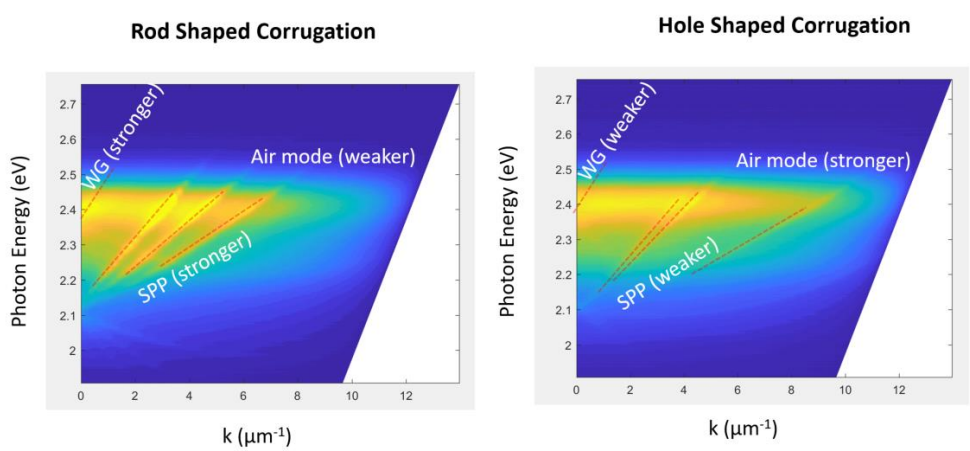

Figure 17. ARES plot for OLEDs fabricated on single crystal substrates. The two corrugated substrates have (left) rod-shaped corrugation and (right) hole-shaped corrugation.

Based on these preliminary ARES study, we further optimized our device structure and reduced thickness MoO_x to be 1 nm. Using the above single crystal patterns, we fabricated corrugated substrates by nano-imprinting a thin layer of NOA 81 epoxy, which has the same index as glass (n = 1.5). Proper planarization with PEDOT is used on the epoxy layer to control the corrugation depth to 80 nm, 65 nm, and 55 nm. After substrate preparation, a 100 nm thick ITO anode is sputtered on the planar and corrugated substrates, and a green OLED stack is fabricated (Fig 18). $Ir(ppy)_2(acac)$ is used as the phosphorescent emitter (emission peak at 520 nm), and Al is used as the top cathode.

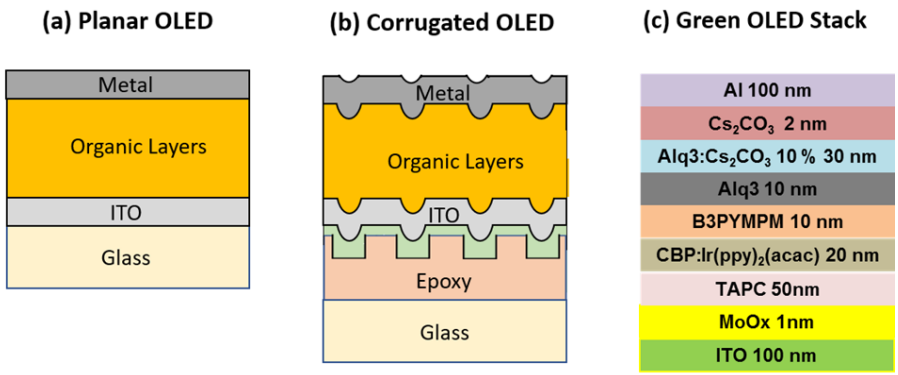

Figure 18. Illustrations of the (a) planar and (b) corrugated OLED structure. (c) The green OLED organic layer stack.

The results for the planar OLED and OLEDs with hole corrugation are shown in Fig 19. The device with corrugation depth 80 nm gave us the best result, which is also analyzed using ARES. Both the planar and hole corrugation OLED have a low leakage current. With the optimized charge balance, the planar device EQE is improved from 24% to 27%, the corresponding current efficiency is 90 cd/A. Hole corrugated device with 80 nm corrugation depth shows an EQE of 33%, which is 22% higher than the planar device; the corresponding current efficiency is 120 cd/A, which is 32% higher than the planar device. When a macrolens is attached on to the device to extract substrate mode, the corrugated device efficiency is improved to 63%. The overall enhancement by combining corrugation with a macrolens is 2.6 times.

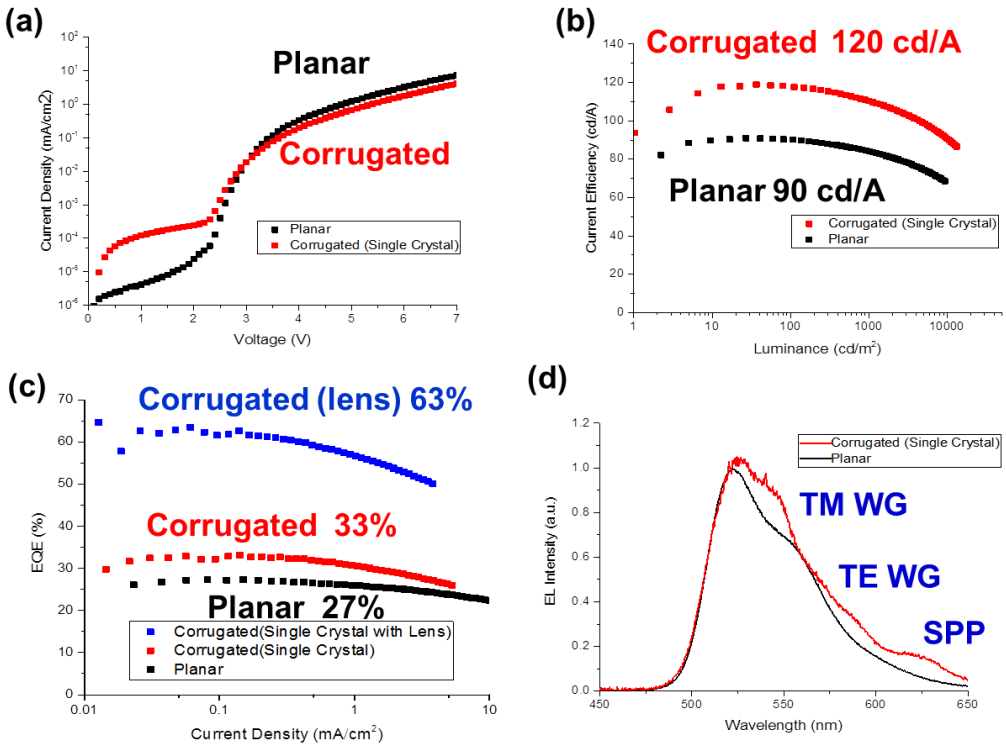

Figure 19. (a) Current density (b) current efficiency (c) EQE plots of planar OLED, corrugated OLED on hole corrugations (d) EL spectra

Corrugated Device by Varying Corrugation Depth

Using ARES measurements, we compared the air modes for planar and hole-corrugated devices with different corrugation depth in Fig 20. The planar device has a uniform and featureless air mode. The corrugated devices all show clear TM waveguided mode and SPP mode features. TE waveguided mode feature is relatively weak and too close to the SPP mode thus difficult to distinguish. The intensity of the diffraction features is noticeably stronger when the corrugation depth is increased from 55 nm to 80 nm. The strongest diffraction strength is observed for OLEDs with 80 nm optimized corrugation depth.

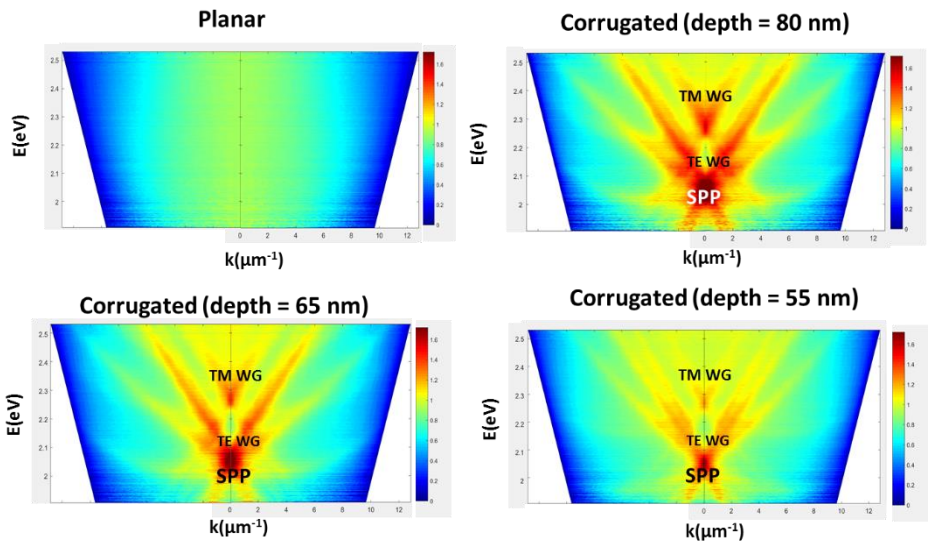

Figure 20. Comparison of air modes for (a) planar OLEDs and corrugated OLEDs on (b) single and (c) poly crystal substrates. The diffraction features are assigned to TM and TE waveguide and SPP modes in corrugated OLEDs.

The reason we don't see strong TE waveguided mode extraction can be attributed to the spatial distribution of modes and the index modulation in the corrugated OLED. Diffraction efficiency is determined by the index modulation strength of an interface. In a corrugated device, this includes both the corrugation depth and the index contrast of the corrugated interface. For the OLED devices we study, glass and PEDOT have the same index of 1.5, ITO has an index of 2.0, organic materials have indices of 1.75, and metal has a very small refractive index in visible wavelengths. Therefore, the metal/organic interface has strong index modulation, while the ITO/glass interface has very weak index modulation.

From the aspect of mode distribution, TM waveguided mode is mainly localized in the organic layers, TE waveguided mode is localized in the ITO layer, and SPP mode is localized on the interface of the metal/organic layers. Although the index modulation between the metal/organic interface is very strong, it cannot affect optical modes of which the electric field is not near the metal surface. Therefore, the corrugated electrode can only affect the SPP and TM waveguided mode, and is powerless against TE waveguided mode because most of its energy is within the ITO layer. TE waveguided mode is mostly diffracted by the interface between ITO and glass, which has an index contrast of 0.5 at $\lambda = 520$ nm. This is the main reason we see very little amount of TE waveguided modes features with our corrugated substrates.

6. Index Contrast Layer for Enhanced Extraction

To further improve the diffraction of waveguided modes, we need stronger index modulation at the glass/ITO corrugation interface. Besides changing corrugation depth and shape, the diffraction efficiency can also be improved by increasing the index contrast at the interface. In our OLED structure, ITO was sputtered onto the corrugated substrates. The largest refractive index difference is between corrugated NOA 81 layer (n = 1.5) and ITO (n ~ 2.0), therefore Δn = 0.5 (Fig 21). With PEDOT as the planarization layer, the index contrast is not affected. However, when a low index material (n = 1.2, for example) is used as the planarization layer, Δn is increased to 0.8.

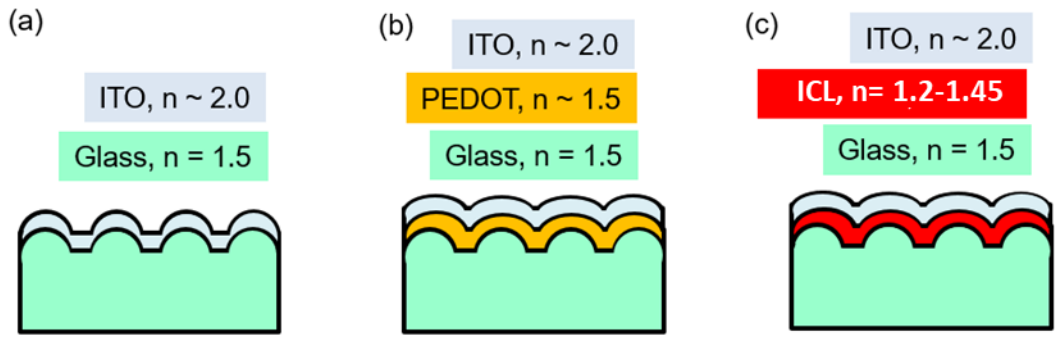

Figure 21. Schematic drawing of corrugated substrate (a) without planarization (b) with PEDOT planarization (c) with low index material planarization

Herein we explored a different approach to fabricate low index layer using commercial solution-processable liquid provided by SBA Materials. The low index layer is spin-coated on glass at a speed of 4000 rpm followed by a two-step annealing method at 150 degrees for 20 mins and 450 degrees for 2 hours. The film has a low index of 1.2 and to have high transparent film above 90% (Fig 22).

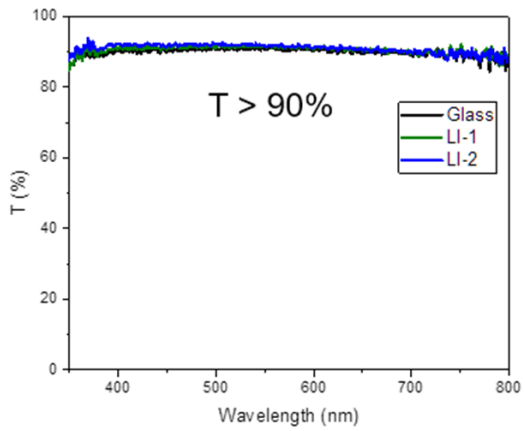

Figure 22. Measured transmittance of (black line) reference glass substrate and glass substrate coated with (green line) single layer and (blue line) double layer low index material. The slight enhancement in transmittance comes from the anti-reflection effect.

Another great advantage of this material is its index tunability. By annealing the film at different temperatures, we can fabricate a set of films, which have refractive indices ranged from 1.5 to 1.2.

Optimized Corrugated Index Contrast Layer Preparation

Using A single crystal pattern, we fabricated corrugated substrates by nano-imprinting a thin layer of UV- curable resin NOA-81 epoxy, which has the same index as glass (n = 1.5) on a glass substrate. A drop of this epoxy is deposited on the glass substrate followed by stamping a corrugation pattern on top of the epoxy. The stamp is then UV treated and removed, leaving a corrugated structure. Partial planarization is done by coating an LI material on the corrugated epoxy structure at 7000 rpm for 40 seconds. This approach is considered to optimize the depth of the substrate and device. The index number of this low index material can be controlled by the annealing temperature and time. Keeping glass transition temperature of NOA epoxy which is 125-150 °C we annealed the low index material coated epoxy substrate at a maximum of 170 °C for 60 minutes to get an index value of 1.38 (Fig 23).

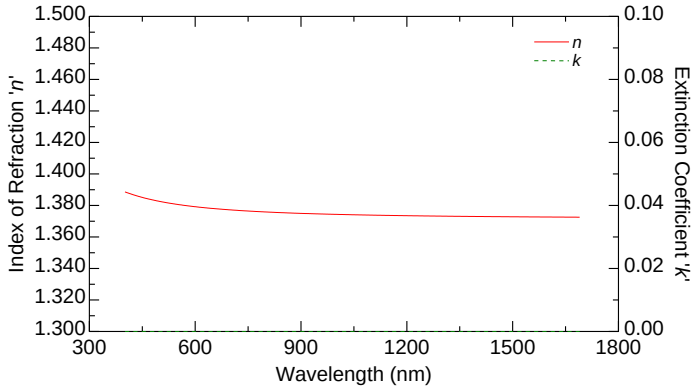

Figure 23. Measured refractive index with ellipsometry for the ICL under 170 °C annealing for 60 minutes. Within the emission wavelength (500 – 650 nm) the refractive indices are between 1.375 – 1.385.

After substrate preparation, a 100 nm thick ITO anode is sputtered on the planar and corrugated substrates, and a green OLED stack is fabricated. $Ir(ppy)_2(acac)$ is used as the phosphorescent emitter (emission peak at 520 nm), and Al is used as the top cathode.

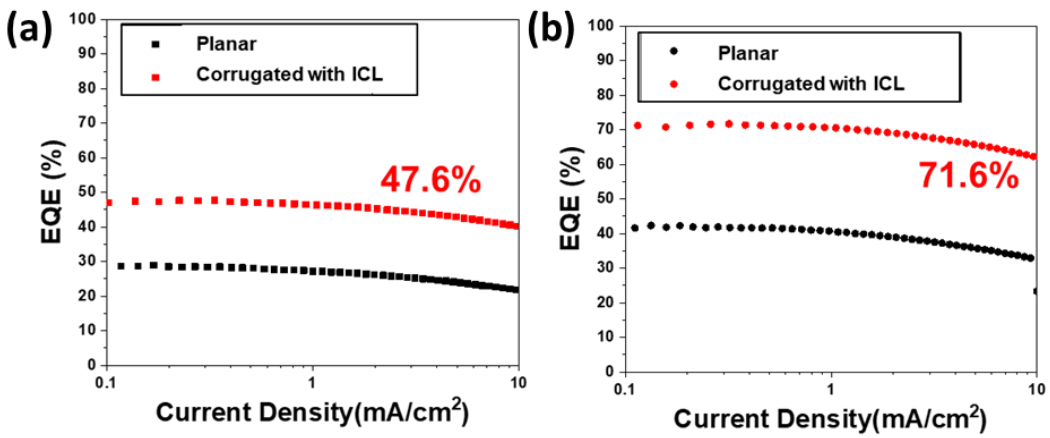

Figure 24. (a) EQE measured with integrating sphere for the reference planar device and corrugated devices with a low index material spin-coated at 7000 rpm with air-gap. (b) EQE with a macrolens attached to extract light trapped in the substrate

Figure 24 shows the EQE data of OLEDs fabricated on planar and corrugated substrates. A higher spin speed reduces the amount of low index material and maintains the corrugation depth.

As a result, the EQE value of the corrugated device is 47.6%. When a macrolens is attached, the efficiency is 71.6%. We attribute the higher efficiency at higher spin speed to the higher corrugation depth at the top Al electrode, deep corrugation pattern and optimized thermal annealing.

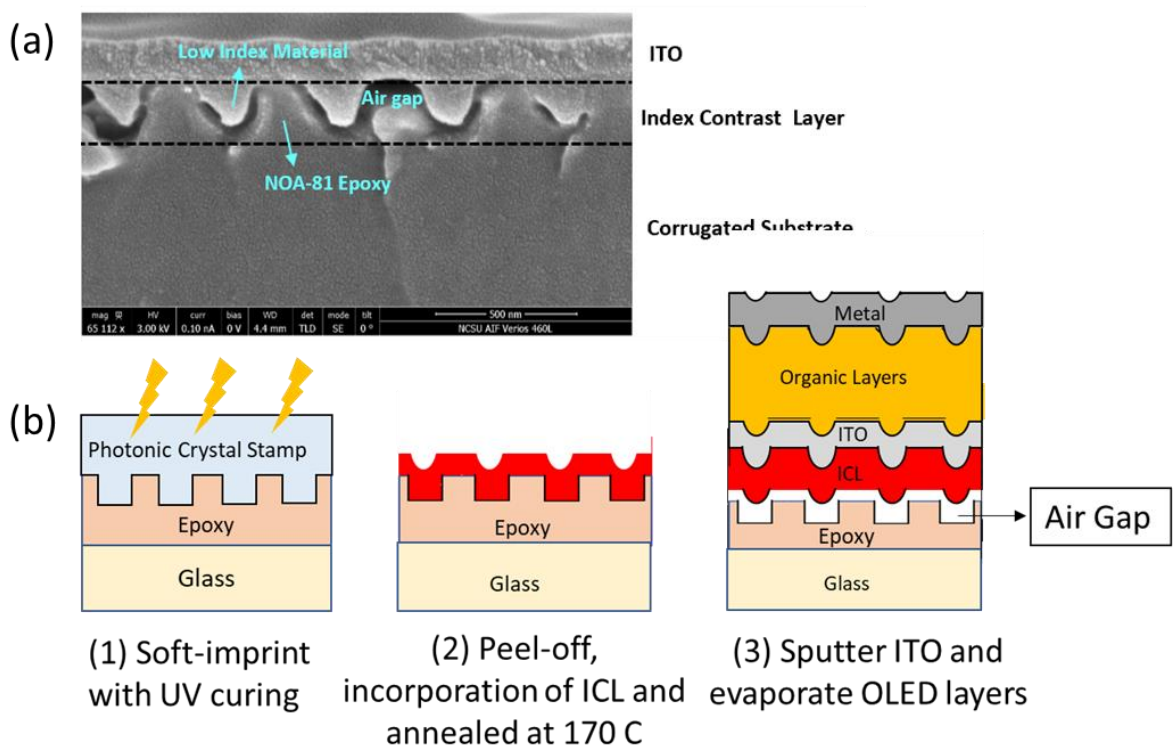

Figure 25. (a) Cross-section SEM image of the index contrast layer on top of the corrugation made with NOA-81 epoxy, (b) fabrication of the air-gap. A clear air gap can be seen between the low index material and the NOA-81 epoxy.

Figure 25 reveals this interesting property of the thermally annealed ICL. The low index material has low viscosity compared to NOA-81 epoxy, which indicates very different thermal properties of the two materials. Upon high-temperature annealing at 170 °C, the two materials shrink at different rates and create air gaps at the interface. Considering the glass transition temperature of NOA 81 epoxy to be 125-150 °C, we could not anneal our substrates above 170 °C. The air gaps (n = 1) create a large refractive index contrast ($\Delta n \sim 1$ between ITO and air gap) and lead to very efficient extraction of trapped light, especially the TE waveguide trapped in the

ITO layer. Along with the optimized depth of corrugation and a low index of 1.38 value, the most efficient device with a macrolens reaches high EQE of 71.6%.

To confirm that the ICL indeed improves the extraction of TE waveguide mode, we conducted ARES measurement on the corrugated OLED with an ICL. The result is compared with a reference planar OLED and a corrugated OLED on the same corrugation pattern but without the ICL (Fig 26). An ARES plot compiles the 181 angular EL spectra (taken from -90° to 90° viewing angles) into a color contour, where stronger EL intensity is represented by red color. ARES plot depicts the air mode distribution of the measured OLED, which supports the EQE data from an optics point of view.

For the planar OLED, the air mode is uniform in intensity (Fig 26a). The corrugated OLEDs have similar backgrounds as the planar OLED but with additional linear features (Fig 26b, 26c). We normalized all the EL spectra with the forward EL spectrum of the planar device, and show the normalized ARES plots in Figure 1d, 1e, 1f. The normalized ARES plots reveal the features from extracted waveguide modes and SPP mode. Without an ICL, the corrugated OLED has very weak TE waveguide feature, stemming from the low index contrast at the ITO/glass interface. With an ICL, the corrugated OLED shows much stronger TE waveguide feature. In addition, both the TM waveguide and the SPP features become stronger as well.

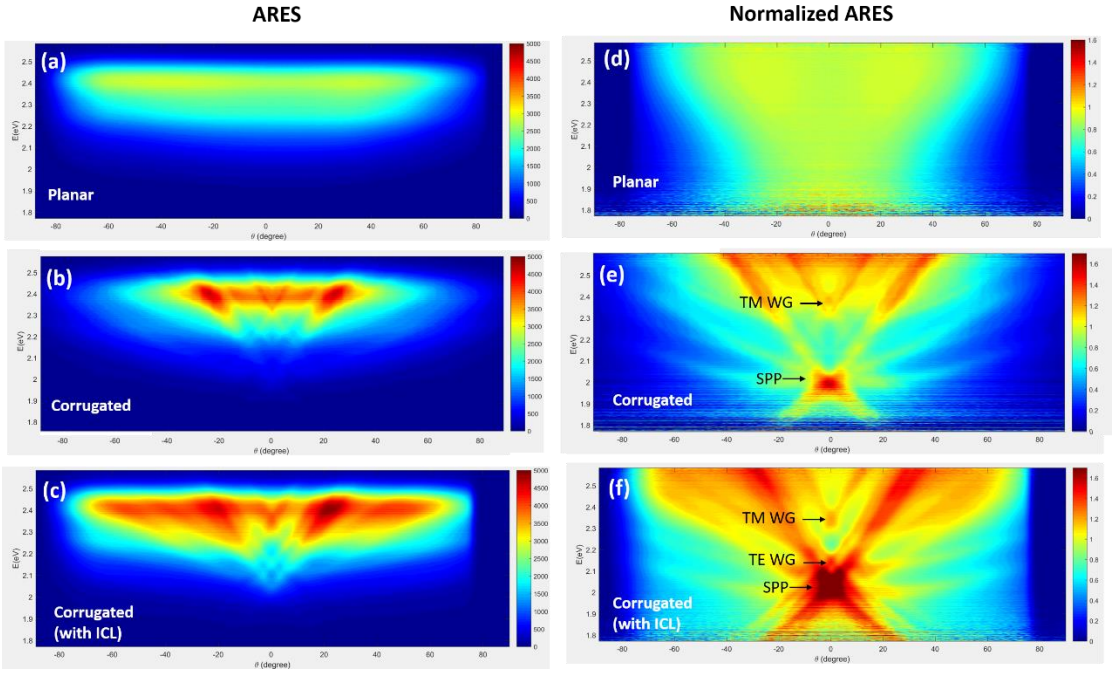

Figure 26. ARES plots of the (a) planar OLED, (b) the corrugated OLED and (c) the corrugated OLED with an index contrast layer, and the corresponding normalized ARES plots in (d)(e)(f).

We notice each extracted mode has 6 sets of linear features, which results from the hexagonal symmetry of the corrugated PhC pattern. The symmetry also results in all the extracted features intercept at $\theta = 0°$ viewing angle. Therefore, we can compare the intensity of each mode using the forward EL spectra (Fig 27). Based on the ARES plot, we attribute the enhancement at 500 – 550 nm to extracted TM waveguide mode, 550-580 nm to extracted TE waveguide mode, and 580 nm – 630 nm to extracted SPP mode. It's clear that all three modes become stronger when an ICL is inserted, with the TE waveguide being improved the most, owing to the enhanced index contrast at the ITO/glass interface. We used FDTD simulation to study the electric field distribution of each mode. While TM waveguide mode and SPP mode are mainly located near the metal surface, their electric field extends to the ITO/glass interface, therefore their extraction efficiencies are also improved by the ICL.

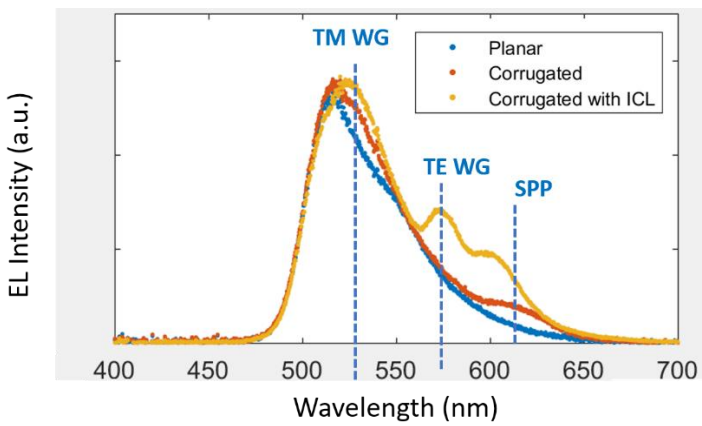

Figure 27. Forward EL spectra comparison of a planar OLED, a corrugated OLED and a corrugated OLED with an index contrast layer. The dashed lines indicate the extraction peaks and the origin of the extracted light.

7. Substrate Mode Extraction with Microlens Arrays

We've demonstrated substrate mode extraction with a macrolens on small pixel (2 mm × 2 mm) OLEDs and observed ×1.6 times enhancement in outcoupling efficiency. For large area OLED panels used for display and lighting applications, the substrate mode extraction is typically done through microlens arrays (MLAs). In this research, we studied MLAs with different geometry, pitch and aspect ratios, and studied how MLAs designs affect the substrate mode extraction efficiency and OLED device quality.

MLAs Geometry and Extraction Efficiency

We first studied linear gratings obtained from 3M company with a 25 μm pitch (Figure 28(1)). The grating shows only ×1.15 times enhancement in outcoupling efficiency. We performed ARES measurement parallel and perpendicular to the grating grooves separately, and found the parallel case shows the exact same air mode as without any MLAs attached, while the perpendicular case shows multiple ripples in the air mode. This indicates only light travelling normal to the direction of the grating grooves is affected. This places a limit to the extraction efficiency and explains the low enhancement amount from the MLAs.

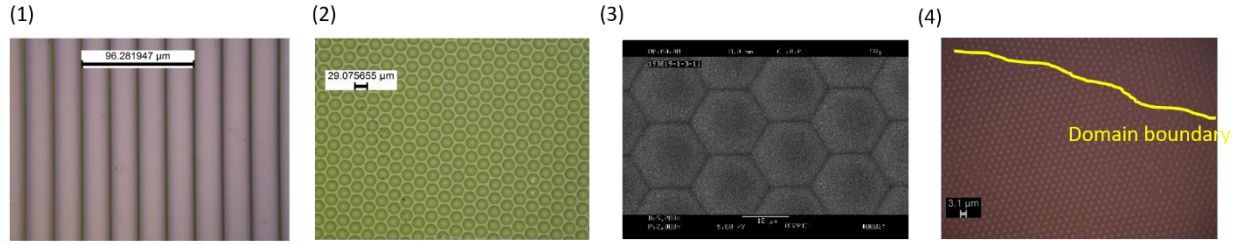

Figure 28 Microscopic image of MLAs with geometries used in this study. (1) Linear gratings, (2) hexagonal close-packed MLAs, (3) honeycomb MLAs, (4) polycrystalline MLAs

To address this problem, we use MLAs with hexagonal close-packed (HCP) lattice, and half-spherical lens units to extract light traveling in all directions (Figure 28(2)). We compared MLAs with different lens diameters (0.4 μm, 0.75 μm, 30 μm, and 250 μm), and found out the sub-micron MLAs had no effect in substrate extraction, indicating the lens diameter should be much larger (over 10 times) than the emitter wavelength to fully utilize the lens effect. In addition, we found the MLAs aspect ratio (height/diameter) needs to be close to 0.5 to be efficient. This can be explained by its resemblance to a macrolens, where light emitted from the sphere center escapes without experiencing TIR.

We also note the fill factor of MLAs on the substrate directly influences extraction efficiency. The HCP MLAs theoretically have 91% fill factor, but due to the spacing between the MLAs, the actual fill factor is around 70%. In comparison, a honeycomb structure theoretically allows the highest extraction efficiency due to 100% fill factor (Figure 28(3)). We obtained honeycomb MLAs from Holographix Inc. with a diameter of 16 μm, an aspect ratio of 0.5. This optimized structure results in ×1.38 times enhancement in device outcoupling efficiency.

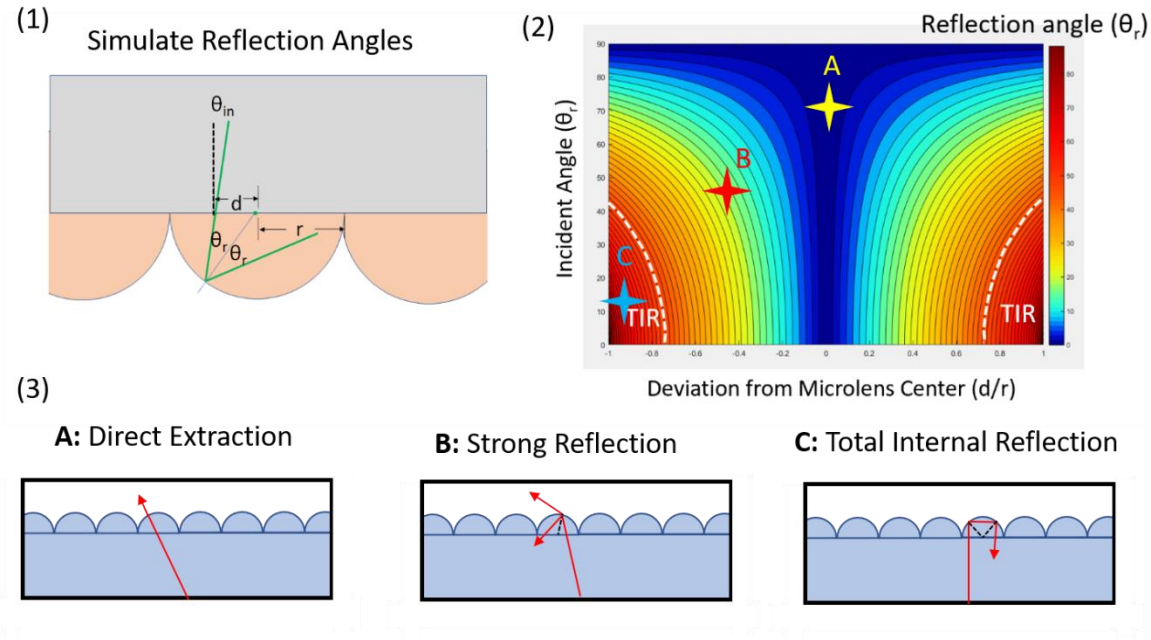

Figure 29. (1) A beam of light hits the glass/MLAs interface with an incident angle of θ_{in}, at a spot deviated from the center of microlens unit by d. (2) Simulated reflection angle inside the microlens. The two corners represent light being total internal reflected back to the substrate. (3) Three typical cases of light beams striking the MLAs and the individual light path.

We then use optical simulation to explain the efficiency gap between a macrolens and the honeycomb MLAs. The simulation considers light beams incident on the interface between the glass substrate and MLAs (Figure 29). Because the OLED device is much large than a single microlens unit, the spot of incidence is random, and the incident angle ranges from -90° to 90°. We simulate the reflection angle at the MLAs/air interface. We found only light striking the microlens center can escape to the air without strong reflection (case A), and as the light beam deviates from the microlens center, stronger reflection (case B) or TIR (case C) occurs which redirects light towards the metal surface, causing strong absorption. Thus, the overall extraction efficiency of MLAs is lower than a macrolens.

Homogeneous Emission with Poly Crystal MLAs

For lighting purpose, directional emission should be minimized for best light quality. When the single crystal HCP MLAs are attached to the substrate, we observed directional emission from the OLED pixel (Figure 30). This is due to the diffraction of substrate mode by the single crystalline hexagonal lattice. We eliminate this issue using polycrystalline MLAs fabricated by a colloidal assembly. In brief, we disperse 3 μm silica spheres to create a mono-layer with polycrystal patterns. We then drop cast PDMS mixture on the mono-layer to replicate the pattern. Later the silica spheres are removed using optical adhesive, leaving a PDMS stamp with the polycrystal MLAs pattern that can be used multiple times for imprinting.

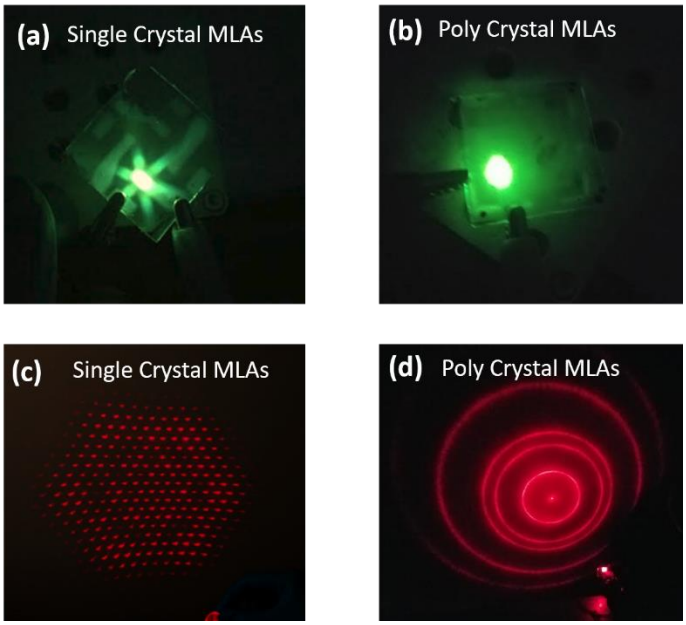

Figure 30. Picture of an operating OLED pixel attached with (a) single crystal MLAs and (b) poly crystal MLAs with 3 μm spheres. (c) and (d) are the corresponding diffraction pattern projected on the wall using a 632 nm red laser source.

The diffraction patterns of the single crystal MLAs and polycrystal MLAs are compared in Figure 30. A beam of red laser (λ = 632 nm) is cast on the substrate and projects a diffraction pattern on the wall. The single crystal MLAs create ordered hexagonal patterns corresponding to the hexagonal lattice, indicating the diffraction is stronger at discrete angles. The polycrystal MLAs create concentric ring patterns, indicating the diffraction is isotropic with no azimuthal angle dependence. We further confirm this with the microscopic image of the MLAs (Figure

28(4)). The polycrystal MLAs have a domain in the size of 10 ~ 100 μm. Within each domain, the lens units follow the HCP lattice for high fill factor, but the entire MLAs sheet has no preferable orientation, which contributes to the homogeneous emission.

Reduce Color Shift from Corrugated OLED with MLAs

Another important function of MLAs is to reduce the color shift caused by the corrugated substrate. We calculate the CIE coordinates at each viewing angle from the ARES measurement, and compare the color shift in planar and corrugated OLEDs in Figure 31. For the planar device, the CIE coordinate shift from 0° to 60° is $\Delta CIE_{x,y}$ = (-0.038, 0.020). For the corrugated device, $\Delta CIE_{x,y}$ = (-0.070, 0.041). The much larger color shift in the corrugated OLED is related to the directional emission from waveguide and SPP mode. Due to the dispersion relation of waveguide and SPP modes, longer wavelength light is extracted to lower angles, and shorter wavelength light is extracted to larger angles, which contribute to the spectrum blue shift. To alleviate this problem, we apply poly crystal MLAs on the substrate to randomize the directional emission. The short and long wavelength light is blended together in all angles, and the spectrum distortion is minimized across all angles. As a result, the color shift for the planar device with MLAs is $\Delta CIE_{x,y}$ = (-0.022, 0.008), and for the corrugated device with MLAs is $\Delta CIE_{x,y}$ = (-0.013, 0.003), negligible to the human eye.

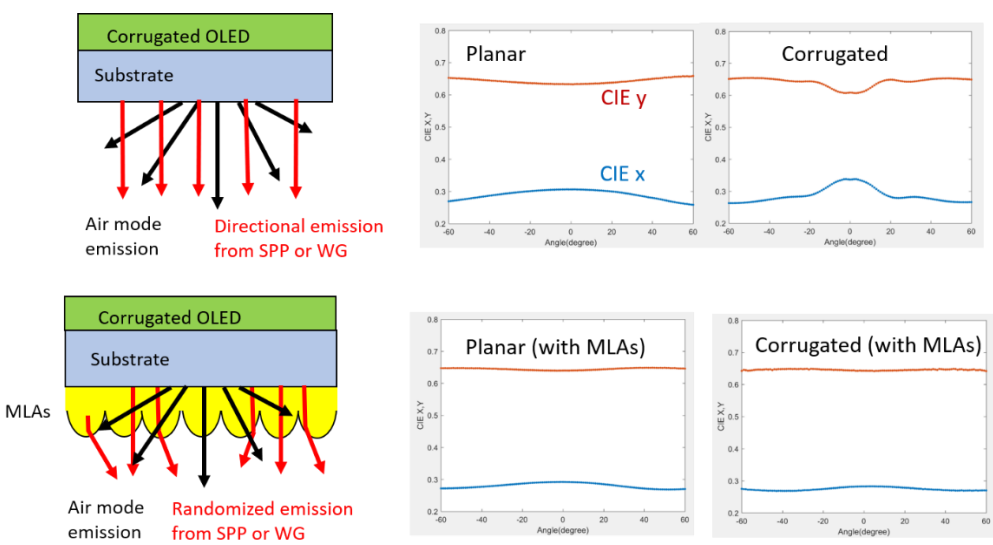

Figure 31. CIE coordinate shift for planar OLED, corrugated OLED with ICL, and the two devices after applying poly crystal MLAs.

In summary, we compared single crystal MLAs and polycrystal MLAs for substrate mode extraction. Polycrystal MLAs are more advantageous for lighting applications due to the isotropic emission profile, which eliminates the directional emission seen in the single crystal MLAs. We also demonstrate MLAs can be used as a diffuser to reduce the color shift caused by corrugated substrates. With these improvements, the design of corrugated OLED with polycrystal MLAs become more suitable for general lighting applications.

8. Conclusion

We summarize the key conclusions in this study:

(1) OLED layers fabricated through sputtering and thermal evaporation can preserve the corrugated profile. A large corrugation depth (~150 nm) results in strong diffraction but also causes strong local electric field which leads to charge imbalance and leakage current. Solution-processed layers (e.g. PEDOT: PSS) can partially planarize the corrugation profile, useful for controlling the corrugation depth.

(2) The EQE enhancement using a corrugated substrate comes from the extraction of waveguide modes and SPP mode. The corrugation acts as a Bragg grating and reduces the in-plane wavevector of trapped light, diffracting it towards air mode. Due to the dispersion of trapped light, the corrugated OLEDs typically show strong color shift at different viewing angles.

(3) TM waveguide mode and SPP modes are mainly distributed near the metal surface, which can be efficiently extracted by the corrugated metal electrode; TE waveguide mode is trapped in the ITO layer, thus requires strong diffraction at the ITO/glass interface to be extracted. By inserting an index contrast layer (ICL) between ITO and glass, the index contrast at this interface is enhanced, TE waveguide mode is significantly improved. TM waveguide mode and SPP modes extraction is also improved due to the electric field distribution extending towards this interface.

(4) MLAs have lower substrate mode extraction efficiency than a macrolens due to undesired total internal reflection from pixel area that’s not at the microlens center. High-efficiency MLAs should have high fill factor (e.g. honeycomb structure) and sufficient height/diameter ratio. The directional emission and color shift caused by the corrugated substrate can be eliminated by attaching poly crystal MLAs as a diffuser.

(5) We demonstrated over 70% EQE can be obtained in a corrugated OLED with efficient substrate mode extraction, improved diffraction strength, and well-tuned electrical properties. We demonstrate ARES as a powerful instrument in the research of OLED light outcoupling efficiency.

We believe this project helps the OLED community understand light extraction from the aspect of thin film optical modes and propel the development of OLED lighting.